NONLINEAR BIFURCATIONS OF DAMPED VISCO-ELASTIC PLANAR BEAMS UNDER SIMULTANEOUS GRAVITATIONAL AND FOLLOWER FORCES

Angelo Luongo
Dipartimento di Ingegneria delle Strutture,
delle Acque e del Terreno
Università degli studi dell'Aquila
Italy
angelo.luongo@univaq.it

Francesco D'Annibale
Dipartimento di Ingegneria delle Strutture,
delle Acque e del Terreno
Università degli studi dell'Aquila
Italy
francesco.dannibale@univaq.it

Abstract

The mechanical behavior of a non-conservative non-linear beam, internally and externally damped, undergoing codimension-1 (static or dynamic) and codimension-2 (double-zero) bifurcations, is analyzed. The system consists of a purely flexible, planar, visco-elastic beam, fixed at one end, loaded at the tip by a follower force and a dead load, acting simultaneously. An integro-differential equation of motion in the transversal displacement, with relevant boundary conditions, is derived. Then, the linear stability diagram of the trivial rectilinear configuration is built-up in the space of the two loading parameters. Emphasis is given to the role of the two damping coefficients on the critical scenario. Attention is then focused on the double-zero bifurcation, for which a post-critical analysis is carried out without any *a-priori* discretization. An adapted version of the Multiple Scale Method, based on a fractional series expansion in the perturbation parameter, is employed to derive the bifurcation equations. Finally, bifurcation diagrams and bifurcation charts are evaluated, able to illustrate the system behavior around the codimension-2 bifurcation point.

Key words

Bifurcations; Damping effects on stability; Non-conservative loads; Multiple scale method; Visco-elastic beam

1 Introduction

Stability of columns subjected to follower forces, after the pioneering paper by [Beck, 1952], have recently attracted the attention of many researchers, particularly in aerospace, where tangential forces are produced by jets and rocket motors [Ryu, Katajama and Sugiyama, 1998], [Langthjem and Sugiyama, 2000]. In many studies, damping is mainly considered as an *external* cause, resulting from the interaction occurring between the structure and the surrounding air (see, e.g. [Detinko, 2003], where both damping forces and couples acting on a tip mass were taken into account). However, damping is also due by an *internal* dissipation of the material, to be modelled by a proper rheological model. A general treatment of the effect of distributed, internal and external small dampings, on the linear stability of a continuous beam under non-conservative loads, can be found in [Kirillov and Seyranian, 2005].

Stability is strongly influenced by damping, which is responsible of a well-known phenomenon, called "the destabilization paradox", according to which the loss of stability of a non-conservative system with vanishingly small damping occurs at a load significantly lower than the critical value relevant to the undamped system. This problem was firstly studied by Ziegler [Ziegler, 1952] and subsequently observed in many non-conservative mechanical systems, [Bolotin and Zhinzher, 1969], [Andreichikov and Yudovich, 1974], [Denisov and Novikov, 1975], [Seyranian, 1990], [Kirillov, 2004].

Follower forces can also act simultaneously to gravitational forces, as for example analyzed in [Langthjem and Sugiyama, 2000], [Adali, 1982], this interaction resulting in richer bifurcation scenarios.

All previous studies have been devoted to analyze the *linear* stability behaviour of systems. However, *nonlinear* systems have also been investigated in the framework of general bifurcation theory [Troger and Steindl, 1991], [Luongo, Di Egidio and Paolone, 2002], mostly under purely non-conservative forces [Troger and Steindl, 1991]. Therefore, it seems interesting, to investigate nonlinear systems under both types of forces, and in presence of both types of damping, in order to analyze the mutual interactions.

In this paper non linear bifurcations of beams, internally and externally damped, loaded by a gravitational

and a follower force acting simultaneously, are studied. The paper is thus organized. In Section 2 the equations of motions are derived. In Section 3 the eigenvalue problem is addressed for the linearized system and its adjoint. In Section 4 the linear stability problem is studied in the parameter space and the critical scenario is depicted, by focusing the attention on the effects of damping. In Section 5 a post-critical analysis around a double-zero bifurcation point is carried out. An adapted version of the Multiple Scale Method is used, which is based on a fractional series expansion in terms of the perturbation parameter, similarly to the analysis carried out in [Luongo and Di Egidio, 2005], [Di Egidio, Luongo and Paolone, 2007], [Luongo and Di Egidio, 2006]. The bifurcation equations are derived and numerically studied to built-up equilibrium paths and bifurcation diagrams. Finally, in Section 6 some conclusions are drawn.

2 Model

A planar beam is considered, fixed at the end A and, simultaneously loaded at the tip B by a follower force of intensity F (tangential to the actual configuration of the beam axis) and by a dead load of intensity P (acting in the direction of the originally rectilinear axis, Fig. 1). The material behavior of the beam obeys to the Kelvin-Voigt rheological model, with elastic modulus E and viscous coefficient η (acting as an internal damping); moreover, the beam is considered to lie on a purely viscous linear soil of constant c (simulating the external damping). The beam is assumed to be inextensible and shear-indeformable, Formulation closely follows the procedure of [Luongo and Di Egidio, 2005], where a similar system was considered, with, however, no dead load nor internal damping, but a lumped visco-elastic device.

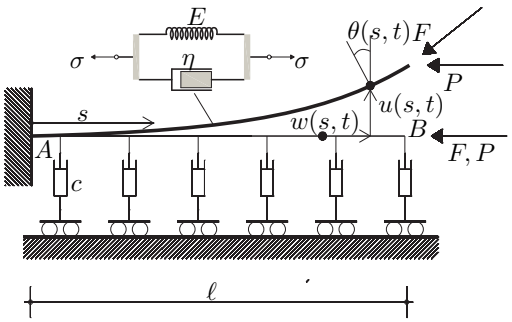

Figure 1. Visco-elastic beam on viscous soil under follower force and dead load: model and displacements.

The actual configuration of the beam is described by the transversal displacement field $u(s,t)$, the longitudinal displacement $w(s,t)$ of the beam axis, and, moreover, the rotation of the section $\vartheta(s,t)$, where $s \in [0,\ell]$ is a curvilinear abscissa and t is the time. The three displacements, however, are not independent, because of the internal constraints, expressing no shear and no stretching, respectively:

$$\sin(\vartheta) = u', \quad \varepsilon := \sqrt{(1+w')^2 + u'^2} - 1 = 0 \quad (1)$$

where a dash denotes differentiation with respect to s. The curvature $\kappa(s,t)$ is assumed as the (unique) strain measure; from Equation (1_1) it follows that:

$$\kappa := \vartheta' = \frac{u''}{\sqrt{1-u'^2}} \quad (2)$$

The equations of motion are derived by the generalized Hamiltonian principle, by introducing the constraint equation (1_2) by a Lagrangian multiplier $N(s,t)$, having the meaning of (reactive) axial force. The variational principle reads:

$$\begin{aligned}\delta H = \int_{t_1}^{t_2}\int_0^{\ell} [m(\dot{u}\delta\dot{u} + \dot{w}\delta\dot{w}) - EI\kappa\delta\kappa - \eta I\dot{\kappa}\delta\kappa + \\ -c\dot{u}\delta u - \delta(N\varepsilon)]\, ds dt + \int_{t_1}^{t_2} [(P + F\cos(\vartheta_B))\,\delta w_B + \\ -F\sin(\vartheta_B)\,\delta u_B]\, dt = 0, \quad \forall(\delta u, \delta w, \delta N)\end{aligned} \quad (3)$$

where EI is the flexural stiffness of the beam, a dot denotes time-differentiation, and the index B evaluation at $s = \ell$. By using Equation (1_1) to eliminate the rotation $\vartheta(s)$, expanding $u(s)$ in Taylor series, the equations of motion, corrected up to the third-order, are derived. By introducing the following non-dimensional quantities:

$$\begin{aligned}&\tilde{t} = \omega t,\ \ \tilde{s} = s/\ell,\ \ \tilde{u} = u/\ell,\ \ \tilde{w} = w/\ell,\\ &\tilde{N} = N/m\ell^2\omega^2,\ \ \omega^2 = EI/m\ell^4,\ \ \alpha = \eta\omega/E,\\ &\beta = c\omega\ell^4/EI,\ \ \mu = F\ell^2/2EI,\ \ \nu = P\ell^2/2EI\end{aligned} \quad (4)$$

omitting the tilde symbol, and still denoting by dashes and dots differentiations with respect non-dimensional quantities, the equations read:

$$\begin{aligned}\ddot{u} + u^{\mathrm{IV}} + \left[u'(u'u'')'\right]' + \alpha\dot{u}^{\mathrm{IV}} + \\ +\alpha\left\{\left[u'(u'u'')'\right]'\right\}^{\bullet} + \beta\dot{u} - (Nu')' = 0\\ \ddot{w} - N' = 0\\ w' + \frac{u'^2}{2} = 0\end{aligned} \quad (5)$$

with the relevant boundary conditions, of geometrical type:

$$w_A = 0,\ \ u_A = 0,\ \ u'_A + \frac{1}{6}u'^3_A = 0 \quad (6)$$

and mechanical type:

$$\begin{aligned} N_B + 2\mu\left(1-\frac{u_B'^2}{2}\right) + 2\nu = 0 \\ -\left[\left(u_B''' + u_B''' u_B'^2 + u_B''^2 u_B'\right) - \left(2\mu + N_B\right) u_B' + \right. \\ \left. +\alpha\left(u_B''' + u_B''' u_B'^2 + u_B''^2 u_B'\right)^{\bullet}\right] = 0 \\ \left(u_B'' + u_B'' u_B'^2\right) + \alpha\left(u_B'' + u_B'' u_B'^2\right)^{\bullet} = 0 \end{aligned} \tag{7}$$

In deriving Eqs. (5)-(7), N' was considered as a second-order quantity, in accordance with Eqs. ($5_{2,3}$), so that terms as $N'u'^2$ were neglected.

The longitudinal displacement $w(s,t)$ and the axial force $N(s,t)$ follow from integration of Eqs. ($5_{2,3}$) with the boundary conditions (6_1) and (7_1), namely:

$$\begin{aligned} w &= -\frac{1}{2}\int_0^s u'^2 ds \\ N &= -2\mu\left(1-\frac{u_B'^2}{2}\right) - 2\nu - \frac{1}{2}\int_1^s \left(\int_0^s u'^2 ds\right)^{\bullet\bullet} ds \end{aligned} \tag{8}$$

By substituting Eq. (8_2) in Eq. (5_1) and in the remaining boundary conditions, the following (condensed) equations in the unique variable $u(s,t)$ are finally derived:

$$\begin{aligned} \ddot{u} + u^{\mathrm{IV}} + \left[u'\left(u'u''\right)'\right]' + \alpha\dot{u}^{\mathrm{IV}} + \\ +\alpha\left\{\left[u'\left(u'u''\right)'\right]'\right\}^{\bullet} + 2\left[\mu\left(1-\frac{u_B'^2}{2}\right)+\nu\right]u'' + \\ +\beta\dot{u} + \frac{1}{2}\left[\left(\int_1^s\left(\int_0^s u'^2 ds\right)^{\bullet\bullet} ds\right)u'\right]' = 0 \\ u_A = 0, \quad u_A' + \frac{1}{6}u_A'^3 = 0, \\ -\left[\left(u_B''' + u_B''' u_B'^2 + u_B''^2 u_B'\right) + 2\left(\nu - \mu\frac{u_B'^2}{2}\right)u_B' + \right. \\ \left. +\alpha\left(u_B''' + u_B''' u_B'^2 + u_B''^2 u_B'\right)^{\bullet}\right] = 0, \\ \left(u_B'' + u_B'' u_B'^2\right) + \alpha\left(u_B'' + u_B'' u_B'^2\right)^{\bullet} = 0 \end{aligned} \tag{9}$$

They are of integro-differential type and contain cubic nonlinearities only. It should be noticed that linearization of the geometrical conditions does not entail any error at this order.

In view of further developments, it is convenient to recast Eqs. (9) in an operator form, in which the mechanical boundary conditions are appended to the field equations [Luongo and Di Egidio, 2005]. The problem accordingly reads:

$$\begin{aligned} \mathbf{M}\ddot{\mathbf{u}} + \mathbf{C}\dot{\mathbf{u}} + \mathbf{K}\mathbf{u} = \mathbf{n}\left(\left(\mathbf{u},\dot{\mathbf{u}}\right)^3\right) \\ \mathbf{g}\mathbf{u} = \mathbf{0} \end{aligned} \tag{10}$$

where:

$$\mathbf{u} := \begin{Bmatrix} u \\ u_B \\ u_B' \end{Bmatrix}, \ \mathbf{M} := \begin{bmatrix} 1&0&0 \\ 0&0&0 \\ 0&0&0 \end{bmatrix}, \ \mathbf{C} := \begin{bmatrix} \beta+\alpha D^4 & 0&0 \\ -\alpha D_B^3 & 0&0 \\ \alpha D_B^2 & 0&0 \end{bmatrix},$$

$$\mathbf{g}\mathbf{u} := \begin{Bmatrix} u_A \\ u_A' \end{Bmatrix}, \ \mathbf{K} := \begin{bmatrix} D^4 + 2\left(\mu+\nu\right)D^2 & 0&0 \\ -D_B^3 - 2\nu D_B^1 & 0&0 \\ D_B^2 & 0&0 \end{bmatrix},$$

$$\mathbf{n}\left(\left(\mathbf{u},\dot{\mathbf{u}}\right)^3\right) := \begin{Bmatrix} -\left[u'\left(u'u''\right)'\right]' + \mu u_B'^2 u'' + \\ -\alpha\left\{\left[u'\left(u'u''\right)'\right]'\right\}^{\bullet} + \\ -\frac{1}{2}\left[\left(\int_1^s\left(\int_0^s u'^2 ds\right)^{\bullet\bullet} ds\right)u'\right]' \\ u_B''' u_B'^2 + u_B''^2 u_B' - \mu u_B'^2 u_B' + \\ +\alpha\left(u_B''' u_B'^2 + u_B''^2 u_B'\right)^{\bullet} \\ -u_B'' u_B'^2 - \alpha\left(u_B'' u_B'^2\right)^{\bullet} \end{Bmatrix} \tag{11}$$

In Equations (10), (11) $\mathbf{M}$, $\mathbf{C}$ and $\mathbf{K}$ are the mass, damping and stiffness operators, respectively, acting on the vector $\mathbf{u} \in \tilde{\mathbb{H}}$, with $\tilde{\mathbb{H}} := \mathbb{H} \oplus \mathbb{R}^2$, which collects the field displacement u and the displacement and its spatial derivative evaluated at the end B; $\mathbf{n}((\mathbf{u},\dot{\mathbf{u}})^3)$ is the vector of nonlinearities (which are cubic homogeneous forms in their arguments and their spatial derivatives and integrals), both in the domain and at the boundary B; $\mathbf{g}\mathbf{u}$ is the vector of the constrained displacements at the end A; moreover $D^n := \partial^n/\partial s^n$, $D_B^n := \partial^n/\partial s^n|_B$. Equations (10) are then rewritten in the following state-form:

$$\begin{aligned} \mathbf{B}\dot{\mathbf{U}} = \mathbf{A}\mathbf{U} + \mathbf{N}\left(\mathbf{U}^3\right) \\ \mathbf{G}\mathbf{U} = \mathbf{0} \end{aligned} \tag{12}$$

where:

$$\begin{aligned} \mathbf{U} := \begin{Bmatrix} \mathbf{u} \\ \mathbf{v} \end{Bmatrix}, \mathbf{v} := \begin{Bmatrix} \dot{u} \\ \dot{u}_B \\ \dot{u}_B' \end{Bmatrix}, \ \mathbf{B} := \begin{bmatrix} \mathbf{I} & \mathbf{0} \\ \mathbf{0} & \mathbf{M} \end{bmatrix}, \\ \mathbf{A} := \begin{bmatrix} \mathbf{0} & \mathbf{I} \\ -\mathbf{K} & -\mathbf{C} \end{bmatrix}, \ \mathbf{N}\left(\mathbf{U}^3\right) := \begin{Bmatrix} \mathbf{0} \\ \mathbf{n}\left(\mathbf{U}^3\right) \end{Bmatrix}, \\ \mathbf{G}\mathbf{u} := \begin{Bmatrix} u_A \\ u_A' \end{Bmatrix} \end{aligned} \tag{13}$$

in which $\mathbf{v} := \dot{\mathbf{u}}$ is the velocity field, and $\mathbf{U} \in \tilde{\mathbb{H}}^2$ the state-vector.

3 Eigenvalue analysis

Bifurcation analysis calls for evaluation of the (right) eigenvalues and eigenvectors of the equations of motion (12). Since the problem is not self-adjoint, also the (left) eigenvectors of the adjoint problem must be determined. The procedure, detailed in [Luongo and Di Egidio, 2005], is here briefly resumed.

3.1 Right and left eigenvalue problems

The equations of motion (12), when linearized, admit the solution $\mathbf{U} = \mathbf{\Phi} e^{\lambda t}$ which leads to the differential eigenvalue problem:

$$\begin{aligned} (\mathbf{A} - \lambda \mathbf{B})\, \mathbf{\Phi} &= \mathbf{0} \\ \mathbf{G}\mathbf{\Phi} &= \mathbf{0} \end{aligned} \tag{14}$$

or, equivalently:

$$\begin{aligned} \hat{\boldsymbol{\phi}} &= \lambda \boldsymbol{\phi} \\ \mathbf{K}\boldsymbol{\phi} + \mathbf{C}\hat{\boldsymbol{\phi}} + \lambda \mathbf{M}\hat{\boldsymbol{\phi}} &= \mathbf{0} \\ \phi_A = 0, \quad \phi'_A &= 0 \end{aligned} \tag{15}$$

having set $\mathbf{\Phi} := \left\{\boldsymbol{\phi}, \hat{\boldsymbol{\phi}}\right\}^{\mathrm{T}} \in \tilde{\mathbb{H}}^2$, $\boldsymbol{\phi} := \{\phi, \phi_B, \phi'_B\}^{\mathrm{T}} \in \tilde{\mathbb{H}}$ and $\hat{\boldsymbol{\phi}} := \left\{\hat{\phi}, \hat{\phi}_B, \hat{\phi}'_B\right\}^{\mathrm{T}} \in \tilde{\mathbb{H}}$. By introducing the scalar products in $\tilde{\mathbb{H}}$ and $\tilde{\mathbb{H}}^2$, respectively:

$$\begin{aligned} (\boldsymbol{\phi}, \boldsymbol{\psi}) &:= \int_0^1 \bar{\phi}_1(s)\, \psi_1(s)\, ds + \\ &\quad + \sum_{j=2,3} \bar{\phi}_j \psi_j \quad \boldsymbol{\phi}, \boldsymbol{\psi} \in \tilde{\mathbb{H}} \\ \langle \mathbf{\Phi}, \mathbf{\Psi} \rangle &:= \int_0^1 \sum_{i=1,4} \bar{\mathbf{\Phi}}_i(s)\, \mathbf{\Psi}_i(s)\, ds + \\ &\quad + \sum_{j=2,3,5,6} \bar{\Phi}_j \Psi_j \quad \mathbf{\Phi}, \mathbf{\Psi} \in \tilde{\mathbb{H}}^2 \end{aligned} \tag{16}$$

and using the bilinear identity:

$$\langle \mathbf{\Psi}, (\mathbf{A} - \lambda \mathbf{B})\, \mathbf{\Phi} \rangle = \left\langle \left(\mathbf{A}^* - \bar{\lambda} \mathbf{B}^*\right) \mathbf{\Psi}, \mathbf{\Phi} \right\rangle \tag{17}$$

the adjoint eigenvalue problem follows:

$$\begin{aligned} \left(\mathbf{A}^* - \bar{\lambda} \mathbf{B}^*\right) \mathbf{\Psi} &= \mathbf{0} \\ \mathbf{G}^* \mathbf{\Psi} &= \mathbf{0} \end{aligned} \tag{18}$$

also written as:

$$\begin{aligned} \mathbf{K}^* \boldsymbol{\psi} + \bar{\lambda} \hat{\boldsymbol{\psi}} &= \mathbf{0} \\ \hat{\boldsymbol{\psi}} - \mathbf{C}^* \boldsymbol{\psi} - \bar{\lambda} \mathbf{M}^* \boldsymbol{\psi} &= \mathbf{0} \\ \psi_A = 0, \quad \psi'_A &= 0 \end{aligned} \tag{19}$$

in which:

$$\begin{aligned} \mathbf{B}^* &:= \begin{bmatrix} \mathbf{I} & \mathbf{0} \\ \mathbf{0} & \mathbf{M}^* \end{bmatrix}, \ \mathbf{A}^* := \begin{bmatrix} \mathbf{0} & -\mathbf{K}^* \\ \mathbf{I} & -\mathbf{C}^* \end{bmatrix}, \\ \mathbf{G}^* \mathbf{\Psi} &:= \begin{Bmatrix} \psi_A \\ -\psi'_A \end{Bmatrix}, \ \mathbf{M}^* := \begin{bmatrix} 1 & 0 & 0 \\ 0 & 0 & 0 \\ 0 & 0 & 0 \end{bmatrix} = \mathbf{M}, \\ \mathbf{C}^* &:= \begin{bmatrix} \beta + \alpha D^4 & 0 & 0 \\ -\alpha D_B^3 & 0 & 0 \\ \alpha D_B^2 & 0 & 0 \end{bmatrix} = \mathbf{C}, \\ \mathbf{K}^* &:= \begin{bmatrix} D^4 + 2(\mu + \nu) D^2 & 0 & 0 \\ -D_B^3 - 2(\mu + \nu) D_B^1 & 0 & 0 \\ D_B^2 + 2\mu & 0 & 0 \end{bmatrix} \end{aligned} \tag{20}$$

and $\mathbf{\Psi} := \left\{\hat{\boldsymbol{\psi}}, \boldsymbol{\psi}\right\}^{\mathrm{T}}$. It should be noticed that while $\mathbf{M}$ and $\mathbf{C}$ are self-adjoint, $\mathbf{K}$ is not self-adjoint, because of the presence of the follower force at the boundary.

3.2 Generalized eigenvectors associated with a double-zero eigenvalue

The case in which $\lambda = 0$ is a double eigenvalue for Eq (14) (and 18)) is of particular interest in bifurcation analysis (Takens-Bogdanov bifurcation). In this occurrence, there exist only one proper right eigenvector $\mathbf{\Phi}_1 = \{\boldsymbol{\phi}_1, \mathbf{0}\}^{\mathrm{T}}$ and only one proper left eigenvector $\mathbf{\Psi}_2 = \{\mathbf{C}^* \boldsymbol{\psi}_2, \boldsymbol{\psi}_2\}^{\mathrm{T}}$; moreover, they are mutually orthogonal, i.e. $\langle \mathbf{\Psi}_2, \mathbf{\Phi}_1 \rangle = (\mathbf{C}^* \boldsymbol{\psi}_2, \boldsymbol{\phi}_1) = 0$. To complete the right basis, a generalized eigenvector $\mathbf{\Phi}_2 = \left\{\boldsymbol{\phi}_2, \hat{\boldsymbol{\phi}}_2\right\}^{\mathrm{T}}$ is needed, which is solution to:

$$\begin{aligned} \mathbf{A}\mathbf{\Phi}_2 &= \mathbf{\Phi}_1 \\ \mathbf{G}\mathbf{\Phi}_2 &= \mathbf{0} \end{aligned} \tag{21}$$

or, equivalently:

$$\begin{aligned} \hat{\boldsymbol{\phi}}_2 &= \boldsymbol{\phi}_1 \\ -\mathbf{K}\boldsymbol{\phi}_2 - \mathbf{C}\hat{\boldsymbol{\phi}}_2 &= \mathbf{0} \\ \phi_{2A} = 0, \quad \phi'_{2A} &= 0 \end{aligned} \tag{22}$$

The generalized eigenvector $\mathbf{\Phi}_2$ is not unique, since $\mathbf{A}$ is singular. To select it univocally, a normalization condition must be enforced, e.g. $\phi_{2B} = 0$; once $\mathbf{\Phi}_2$ has been normalized, also $\mathbf{\Psi}_2$ is normalized, by requiring $\langle \mathbf{\Psi}_2, \mathbf{\Phi}_2 \rangle = 1$.

4 Linear stability analysis

4.1 Bifurcation loci

Stability of the trivial, rectilinear configuration of the beam is governed by the linear eigenvalue problem

(10). In extended form, it reads:

$$\begin{aligned}(1+\alpha\lambda)\phi^{\mathrm{IV}}+2(\mu+\nu)\phi''+\left(\lambda^2+\beta\lambda\right)\phi=0\\ \phi_A=0,\ \ \phi'_A=0,\\ -(1+\alpha\lambda)\phi'''_B-2\nu\phi'_B=0,\ \ (1+\alpha\lambda)\phi''_B=0\end{aligned} \tag{23}$$

The field equation (23_1) and the boundary conditions at A lead to the solution:

$$\begin{aligned}\phi(s)=&c_1\left[\cos(ps)-\cosh(qs)\right]+\\ &+c_2\left[\frac{1}{p}\sin(ps)-\frac{1}{q}\sinh(qs)\right]\end{aligned} \tag{24}$$

where

$$\begin{aligned}q^2&:=\frac{\sqrt{(\mu+\nu)^2-(1+\alpha\lambda)(\beta\lambda+\lambda^2)}-(\mu+\nu)}{(1+\alpha\lambda)}\\ p^2&:=\frac{\sqrt{(\mu+\nu)^2-(1+\alpha\lambda)(\beta\lambda+\lambda^2)}+(\mu+\nu)}{(1+\alpha\lambda)}\end{aligned} \tag{25}$$

and $\mathbf{c}:=(c_1,c_2)^{\mathrm{T}}$ are arbitrary constants. It should be noted that factors $1/p,\ 1/q$ have been introduced in Eq. (24), in order it holds even when $p\to 0$ or $q\to 0$. By enforcing boundary conditions at B, two algebraic equations follow:

$$\mathbf{S}_\lambda\mathbf{c}=\mathbf{0} \tag{26}$$

where:

$$\mathbf{S}_\lambda:=\begin{bmatrix}-\left(p^3+p^3\alpha\lambda\right)\sin(p)+ & \left(p^2+p^2\alpha\lambda\right)\cos(p)+\\ +2p\nu\sin(p)+ & -2\nu\cos(p)+\\ +\left(q^3+q^3\alpha\lambda\right)\sinh(p)+ & +\left(q^2+q^2\alpha\lambda\right)\cosh(q)+\\ +2q\nu\sinh(p) & +2\nu\cosh(q)\\ -(1+\alpha\lambda)\left(p^2\cos(p)\right)+ & -(1+\alpha\lambda)(p\sin(p))+\\ -(1+\alpha\lambda)\left(q^2\cosh(q)\right) & -(1+\alpha\lambda)(q\sinh(q))\end{bmatrix} \tag{27}$$

is the "dynamic stiffness matrix" of the system, depending on the eigenvalue λ. This matrix, however, also depends on the *control parameters*, (μ,ν) and the auxiliary parameters (α,β), i.e. $\mathbf{S}_\lambda=\mathbf{S}_\lambda(\mu,\nu;\alpha,\beta)$. The characteristic equation $\det\mathbf{S}_\lambda(\mu,\nu;\alpha,\beta)=0$ supplies the eigenvalues λ as a function of $(\mu,\nu;\alpha,\beta)$. To restate the problem in real variables, the eigenvalues are written as $\lambda=\xi+i\omega$, with $\xi,\omega\in\mathbb{R}$, and then the characteristic equation re-written in the form:

$$f(\xi,\omega;\mu,\nu;\alpha,\beta)+i\,g(\xi,\omega;\mu,\nu;\alpha,\beta)=0 \tag{28}$$

with $f,g\in\mathbb{R}$. For a fixed set of parameter $(\mu,\nu;\alpha,\beta)^{\mathrm{T}}$, the system of two real equations $f=0,\ g=0$ furnishes the unknowns ξ,ω. From a geometrical point of view, for given values of the parameters $(\mu,\nu;\alpha,\beta)$, each of these equations describes a curve in the (ξ,ω)- plane, which intersect each other in an infinite number of points, representing the eigenvalues of the systems.

In order to find the divergence boundary in the control parameter space, the loci $\mathcal{D}$ of the roots $\xi=0,\ \omega=0$ must be found. Since $g(0,0;\mu,\nu;\alpha,\beta)$ is found to vanish identically for any $(\mu,\nu;\alpha,\beta)$, and $f(0,0;\mu,\nu;\alpha,\beta)$ is found to be independent of the damping coefficients α,β, Eq. (28) assumes the following simple form:

$$(\mu+\nu)^{3/2}\left[\mu+\nu\cos\left(\sqrt{2(\mu+\nu)}\right)\right]=0 \tag{29}$$

This equation implicitly defines a multi-branch curve $\mathcal{D}$ on the (ν,μ)-plane.

Hopf bifurcation occurs at the manifold $\mathcal{H}$ of the parameter plane on which $\xi=0,\ \omega\neq 0$, defined by:

$$\begin{cases}f(0,\omega;\mu,\nu;\alpha,\beta)=0\\ g(0,\omega;\mu,\nu;\alpha,\beta)=0\end{cases} \tag{30}$$

These equations, for a given pair of damping coefficients (α,β), implicitly define a multi-branch curve $\mathcal{H}$ in the (ν,μ)-plane, parameterized by the ω-parameter. No closed-form solutions, but only numerical, can be pursued for Eqs. (30).

4.2 Linear stability diagrams

The linear stability diagram of the beam, is depicted in Fig. 2. All quadrants of the (ν,μ)-plane have been displayed, to account for both tensile/compressive forces. Equation (29) (divergence locus) defines a family of curves (independent of damping) labelled with $\mathcal{D}$. Equation (29) also defines an additional straight line $\mathcal{N}$, of equation $\mu=-\nu$, but, as it will be shown ahead, this is *not* a bifurcation locus, since the transversality condition of the eigenvalues is not satisfied on it. Equations (30) (Hopf locus) define a second family of curves labelled with $\mathcal{H}$ (depending on damping). Of this family, the curves relevant to the undamped system ($\alpha=\beta=0$, also referred as *circulatory system*) have been denoted by $\mathcal{H}^u$, and curves relevant to a slightly damped sample system, ($\alpha=0.01,\beta=0.1$) by $\mathcal{H}^d$. Loci $\mathcal{D}$ and $\mathcal{H}$ represent codimension-1 bifurcations. The divergence-locus $\mathcal{D}$ intersects the ν-axis at points $E_1,E_2,\cdots$, each corresponding to an Eulerian critical load, $\nu_{E_1}=\pi^2/8,\ \nu_{E_2}=9\pi^2/8,\cdots$. The Hopf- locus $\mathcal{H}$ intersects the μ-axis at the Beck's loads. Only the lower intersection is depicted in Fig. 2, both for the undamped system, $B_1^u:=(0,10.025)$, and for the damped system, $B_1^d:=(0,6.464)$. Consistently with the destabilizing effect phenomenon, a small amount of damping considerably reduces the critical load.

The Hopf-curves die at intersections with the divergence curves, according to the well-known mechanism

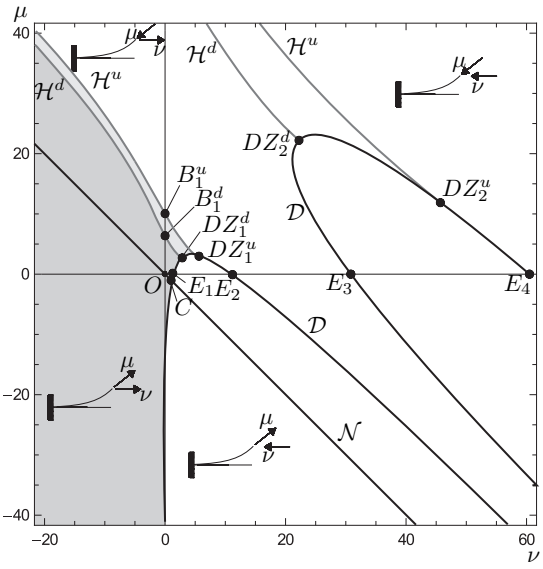

Figure 2. Linear stability diagram for the undamped system ($\alpha, \beta = 0$; u superscript) and a sample damped system ($\alpha = 0.01, \beta = 0.1$; d superscript); $\mathcal{D}$: divergence locus, $\mathcal{H}$: Hopf locus, $\mathcal{N}$: zero-stress locus; E: Eulerian bifurcations; B: Beck's bifurcations; DZ: double-zero bifurcations.

of the double-zero (or Takens-Bogdanov) bifurcation (see for example [Luongo, Paolone and Di Egidio, 2000]). Such codimension-2 bifurcation occurs at points $DZ_1^u := (5.51, 3.02)$, $DZ_2^u := (45.87, 11.76)$, in the undamped case, and $DZ_1^d := (2.88, 2.81)$, $DZ_2^d := (22.26, 22.26)$, in the damped case. For the former, circulatory system, the two loci merge with the same tangent, whereas, in the damped case, they cross each other transversally. The high sensitivity of the double-zero points should be noted, consequent to the large shift of the Hopf loci caused by damping.

The straight line $\mathcal{N}$ represents a one-parameter family of beams unstressed in the undeformed configuration, since the two forces balance themselves when aligned. However, when the beam moves to an adjacent configuration, and due to the different behaviour of the two forces, a (nondimensional) transversal force proportional to the tip rotation rises, namely $V_B := -\mu u'_B$. Since u_B and u'_B are concordant in sign in the resulting static deflection, (a) when $\mu > 0$ (compressive follower force) V_B is opposite to u_B, and therefore is stabilizing; (b) when $\mu < 0$ (tensile follower force), the force is concordant with u_B, and therefore is (potentially) destabilizing. However, for values of $|\mu| < 1$ (corresponding to the $\overline{OC}$ segment in the figure), V_B is smaller than the elastic forces necessary to keep the beam in the deformed configuration, so that the trivial equilibrium is still stable; the opposite occurs for $|\mu| > 1$ (below point C), so that the trivial equilibrium is unstable. Therefore $C := (1, -1)$ is a critical point for this family of systems.

As a final results of the previous analysis, the stable zone of the (ν, μ)-plane is denoted in grey in the figure; it undergoes a contraction when a small damping is added.

The stability diagram of Fig. 2 is zoomed in Fig. 3, to focus the interest on the boundaries of the stable zone and to investigate the behaviour of the eigenvalues around $\mathcal{N}$. Figures $3_{\mathrm{a,b}}$ describe the scenario for the undamped and damped cases, respectively, and give a sketch of the eigenvalues in the different zones. The undamped case is analyzed first (Fig. 3_{a}). Here, the system is (not asymptotically) stable if all its eigenvalues lie on the imaginary axis, as it occurs in the grey zone. The transition through the divergence curve, moving from the left, occurs as follows: a couple of imaginary eigenvalues first collides at zero (on $\mathcal{D}$) and then split into a couple of opposite in sign real eigenvalues. The transition trough the Hopf curve happens as follows: two couples of purely-imaginary eigenvalues moves towards each other, coalesce in double eigenvalues (on $\mathcal{H}$), and then splits again into two couples of complex and conjugate eigenvalues, having opposite real parts. The straight line $\mathcal{N}$, instead, does not affect stability. Indeed, by crossing them in the stable zone, a couple of purely imaginary eigenvalues collides at the origin (on $\mathcal{N}$), then splits again into two purely imaginary eigenvalues. Therefore, no zero eigenvalue passes through the imaginary axis, and therefore no bifurcations occurs. Similarly, by crossing the line in the unstable zone, a couple of opposite in sign real eigenvalues collides at zero (on $\mathcal{N}$), then it splits again into opposite in sign real eigenvalues. At the critical point C, a more degenerate condition occurs, where four eigenvalues coalesce at zero. The eigenvalues of the unstable region, further to the right, are also sketched for low and high values of μ.

When the system is damped (Fig. 3_{b}), (asymptotic) stability requires that all the eigenvalues have negative real parts, while the system is unstable if at least one eigenvalue has positive real part. Loss of stability through divergence and Hopf loci occurs via the classical mechanisms, namely: (a) two stable complex-conjugate eigenvalues first collide on the real axis, then, one of them crosses the imaginary axis at zero (on $\mathcal{D}$); (b) a couple of stable complex conjugate eigenvalues simultaneously crosses the imaginary axis (on $\mathcal{H}$). Again, the $\mathcal{N}$ line does not influence stability, since the mechanism is identical to that of the undamped case. At the critical point C, three eigenvalues coalesce at zero. Eigenvalues in the rightmost region are also indicated.

A parametric study on the influence of both internal (α) and external (β) damping coefficients is then carried out. First, the effect of a single parameter is studied in Figs. $4_{\mathrm{a,b}}$. In Fig. 4_{a} the α coefficient is zeroed, while the β coefficient is varied in a wide range. It is found that, for any value of β, *all the Hopf loci originate from the same double-zero point of the undamped system* $DZ_\beta \equiv DZ_1^u = (5.51, 3.02)$. However, curves modify their shape; in particular, the attack angle with the divergence curve increases from zero for increas-

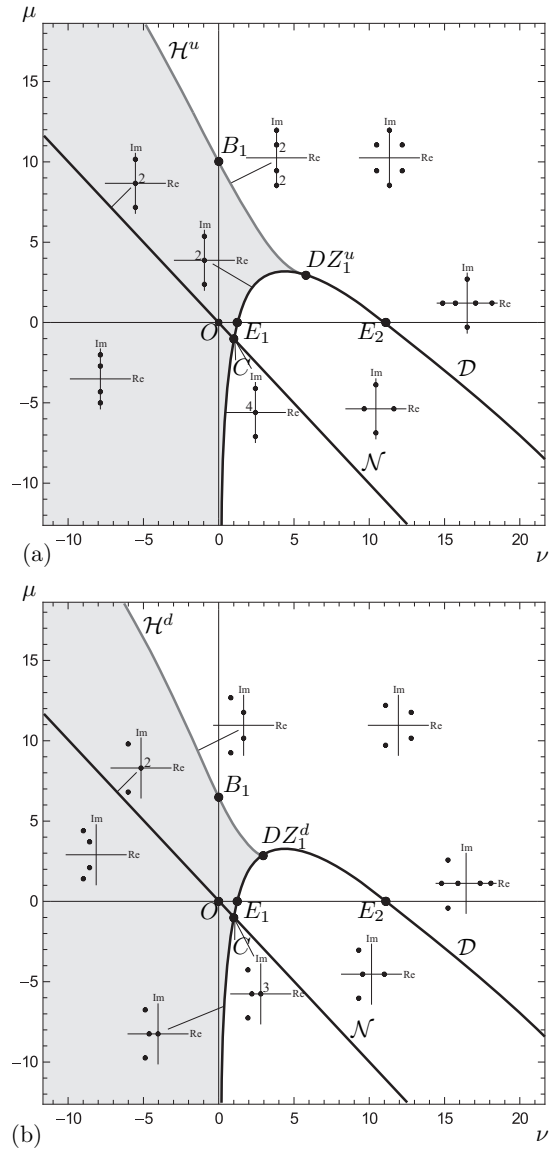

Figure 3. Linear stability diagrams and eigenvalue sketches; (a) undamped system ($\alpha, \beta = 0$); (b) damped system ($\alpha = 0.01$,$\beta = 0.1$).

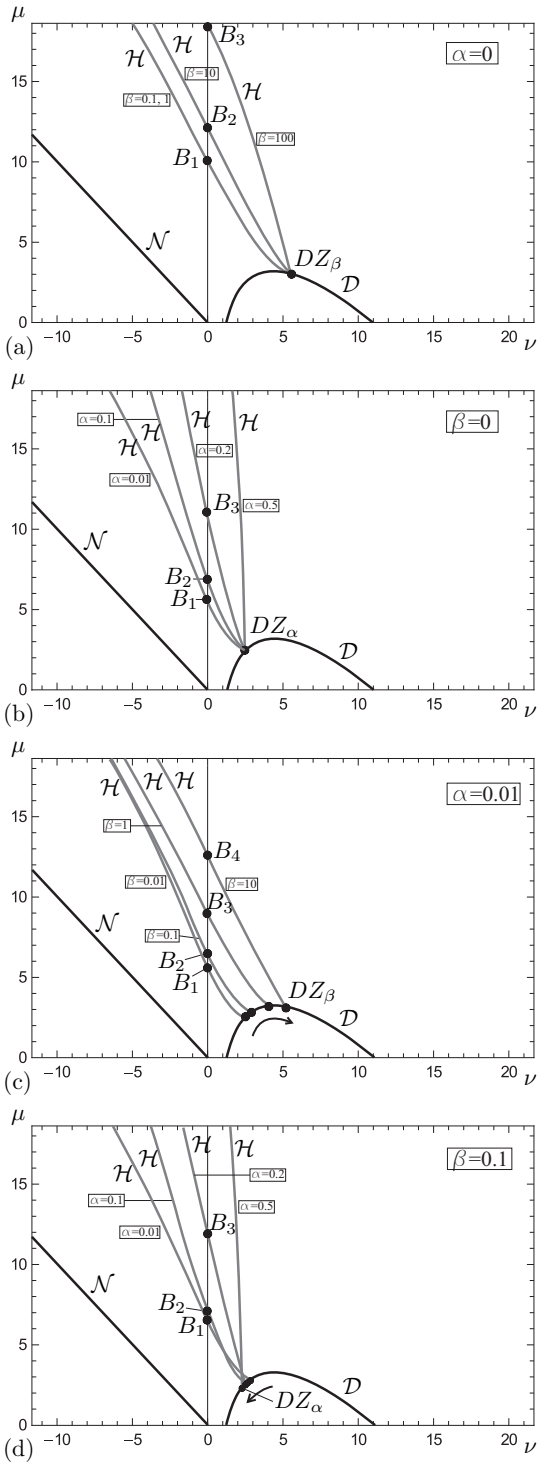

Figure 4. Linear stability diagrams varying damping coefficients for: (a) purely externally damped systems; (b) purely internally damped systems; (c), (d) externally and internally damped systems.

ing β. As a consequence, the Beck's load also increases with β (e.g. $\mu_B = 10.05,\ 12.13,\ 18.60$ when, $\beta = 0.01, 10, 100$ respectively). In Fig. $4_{\rm b}$ β is zeroed, while α is varied. Again, the double-zero point $DZ_\alpha := (2.46, 2.46)$ is found to be independent of the damping value, but *it does not coincide with that of the undamped system*. Moreover, when $\alpha \to 0$, the angle of attack to the divergence curve tends to $\pi/2$, instead of zero. Due to the deformation of $\mathcal{H}$, the Beck's load highly increases with α (e.g. $\mu_B = 5.48,\ 6.82,\ 10.75$ when $\alpha = 0.01,\ 0.1,\ 0.2$, respectively).

To analyze the combined effect of the two parameters, one is kept constant and non-zero, and the other is varied (Fig. $4_{\rm c,d}$). For fixed $\alpha = 0.01$ and increasing β, the scenario of Fig. $4_{\rm c}$ is found. The Hopf locus moves to the right, and the double-zero point tends to DZ_β. Consequently, the Beck's load increases with β (e.g. $\mu_B = 5.61,\ 6.46,\ 8.90,\ 12.60$, when $\beta = 0.01,\ 0.1,\ 1,\ 10$, respectively). For fixed $\beta = 0.1$ and increasing α (Fig. $4_{\rm d}$), the Hopf locus moves to the right and rotates, intersecting the divergence locus at double-zero points tending to DZ_α. Accordingly, the Beck's load increases with α (e.g. $\mu_B = 6.46,\ 7.04,\ 10.99$, when $\alpha = 0.01,\ 0.1,\ 0.2$).

5 Bifurcation analysis around a double-zero point

5.1 Bifurcation equation

A nonlinear bifurcation analysis is carried out around a double-zero bifurcation point. The partial, integro-differential equations (12) are directly attacked (i.e. without introducing any *a-priori* discretization) by an adapted version of the Multiple Scale Method (see also [Luongo and Di Egidio, 2006]).

A perturbation parameter $0 \leqslant \varepsilon \ll 1$, of the order of the response amplitude, is introduced via the rescaling $\mathbf{U}(s,t) = \varepsilon^{1/2}\hat{\mathbf{U}}(s,t)$, where $\mathrm{O}\left(\left\|\hat{\mathbf{U}}(s,t)\right\|\right) = 1$. Increments $\varepsilon\,(\hat{\mu},\hat{\nu})$ of the bifurcation parameters (μ,ν) with respect their bifurcation values (μ_0,ν_0) are introduced, i.e. $\mu = \mu_0 + \varepsilon\hat{\mu}$, $\nu = \nu_0 + \varepsilon\hat{\nu}$, where $\mathrm{O}\,(\hat{\mu}) = \mathrm{O}\,(\hat{\nu}) = 1$. Consequently:

$$\mathbf{K} = \mathbf{K}_0 + \varepsilon\,(\hat{\mu}\mathbf{K}_\mu + \hat{\nu}\mathbf{K}_\nu) + \mathrm{O}\left(\varepsilon^2\mathbf{I}\right) \tag{31}$$

where $\mathbf{K}_\mu$, $\mathbf{K}_\nu$ are the derivatives of $\mathbf{K}$ with respect the parameters. Hats will be omitted ahead for notational convenience. Several independent time scales are defined, namely $t_k := \varepsilon^{k/2}t$, $(k = 0,1,\cdots)$, so that $\mathrm{d}/\mathrm{d}t = \mathrm{d}_0 + \varepsilon^{1/2}\mathrm{d}_1 + \varepsilon\mathrm{d}_2 + \cdots$. The unknowns are expanded in series of fractional powers of ε as:

$$\mathbf{U} = \sum_{k=0,1,\ldots} \varepsilon^{k/2} \begin{Bmatrix} \mathbf{u}_k \\ \mathbf{v}_k \end{Bmatrix} \tag{32}$$

After substitution of the previous expansions in Eqs. (12), a chain of *linear* perturbation equations and relevant boundary conditions follow (hats omitted):

$$\begin{aligned}
\varepsilon^0 &: \begin{cases} \mathrm{d}_0\mathbf{u}_0 - \mathbf{v}_0 = \mathbf{0} \\ \mathbf{M}\mathrm{d}_0\mathbf{v}_0 + \mathbf{K}_0\mathbf{u}_0 + \mathbf{C}\mathbf{v}_0 = \mathbf{0} \\ u_{0A} = 0, \;\; u'_{0A} = 0 \end{cases} \\
\varepsilon^{1/2} &: \begin{cases} \mathrm{d}_0\mathbf{u}_1 - \mathbf{v}_1 = -\mathrm{d}_1\mathbf{u}_0 \\ \mathbf{M}\mathrm{d}_0\mathbf{v}_1 + \mathbf{K}_0\mathbf{u}_1 + \mathbf{C}\mathbf{v}_1 = -\mathbf{M}\mathrm{d}_1\mathbf{v}_0 \\ u_{1A} = 0, \;\; u'_{1A} = 0 \end{cases} \\
\varepsilon &: \begin{cases} \mathrm{d}_0\mathbf{u}_2 - \mathbf{v}_2 = -\mathrm{d}_2\mathbf{u}_0 - \mathrm{d}_1\mathbf{u}_1 \\ \mathbf{M}\mathrm{d}_0\mathbf{v}_2 + \mathbf{K}_0\mathbf{u}_2 + \mathbf{C}\mathbf{v}_2 = -\mathbf{M}\mathrm{d}_2\mathbf{v}_0 + \\ \quad - \mathbf{M}\mathrm{d}_1\mathbf{v}_1 - (\mu\mathbf{K}_\mu + \nu\mathbf{K}_\nu)\,\mathbf{u}_0 + \mathbf{n}\left(\mathbf{U}_0^3\right) \\ u_{2A} = 0, \;\; u'_{2A} = 0 \end{cases} \\
\varepsilon^{3/2} &: \begin{cases} \mathrm{d}_0\mathbf{u}_3 - \mathbf{v}_3 = -\mathrm{d}_3\mathbf{u}_0 - \mathrm{d}_2\mathbf{u}_1 - \mathrm{d}_1\mathbf{u}_2 \\ \mathbf{M}\mathrm{d}_0\mathbf{v}_3 + \mathbf{K}_0\mathbf{u}_3 + \mathbf{C}\mathbf{v}_3 = -\mathbf{M}\mathrm{d}_3\mathbf{v}_0 + \\ \quad - \mathbf{M}\mathrm{d}_2\mathbf{v}_1 - \mathbf{M}\mathrm{d}_1\mathbf{v}_2 - (\mu\mathbf{K}_\mu + \nu\mathbf{K}_\nu)\,\mathbf{u}_1 + \\ \quad + 3\mathbf{n}\left(\mathbf{U}_0^2\mathbf{U}_1\right) \\ u_{3A} = 0, \;\; u'_{3A} = 0 \end{cases}
\end{aligned} \tag{33}$$

The first perturbation equation (33_1) admits the (generating) not-diverging solution:

$$\mathbf{U}_0 \equiv \begin{Bmatrix} \mathbf{u}_0 \\ \mathbf{v}_0 \end{Bmatrix} = a\,(t_1, t_2, \cdots) \begin{Bmatrix} \boldsymbol{\phi}_1 \\ \mathbf{0} \end{Bmatrix} \tag{34}$$

where $\boldsymbol{\Phi}_1 := \{\boldsymbol{\phi}_1, \mathbf{0}\}^{\mathrm{T}}$ is an eigenvector for Eq. (15), and $a(t_0, t_1, \cdots)$ is a real unknown amplitude, which is modulated on the slower time-scales. Whit equations (34), the problem (33_2) reads:

$$\varepsilon^{1/2} : \begin{cases} \mathrm{d}_0\mathbf{u}_1 - \mathbf{v}_1 = -\mathrm{d}_1 a\boldsymbol{\phi}_1 \\ \mathbf{M}\mathrm{d}_0\mathbf{v}_1 + \mathbf{K}_0\mathbf{u}_1 + \mathbf{C}\mathbf{v}_1 = \mathbf{0} \\ u_{1A} = 0, \;\; u'_{1A} = 0 \end{cases} \tag{35}$$

Since the known term belongs to the range of the operator (recall Eq. (22)), Eq. (35) admits the steady solution:

$$\mathbf{U}_1 \equiv \begin{Bmatrix} \mathbf{u}_1 \\ \mathbf{v}_1 \end{Bmatrix} = \mathrm{d}_1 a\,(t_1, t_2, \cdots) \begin{Bmatrix} \boldsymbol{\phi}_2 \\ \boldsymbol{\phi}_1 \end{Bmatrix} \tag{36}$$

in which $\boldsymbol{\Phi}_2 := \left\{\boldsymbol{\phi}_2, \hat{\boldsymbol{\phi}}_2\right\}^{\mathrm{T}} = \{\boldsymbol{\phi}_2, \boldsymbol{\phi}_1\}^{\mathrm{T}}$ is the order-2 generalized eigenvector. With equations (34) and (36), the problem (33_3) reads:

$$\varepsilon : \begin{cases} \mathrm{d}_0\mathbf{u}_2 - \mathbf{v}_2 = -\mathrm{d}_2 a\boldsymbol{\phi}_1 - \mathrm{d}_1^2 a\boldsymbol{\phi}_2 \\ \mathbf{M}\mathrm{d}_0\mathbf{v}_2 + \mathbf{K}_0\mathbf{u}_2 + \mathbf{C}\mathbf{v}_2 = -\mathrm{d}_1^2 a\mathbf{M}\boldsymbol{\phi}_1 + \\ \quad - a\,(\mu\mathbf{K}_\mu + \nu\mathbf{K}_\nu)\,\boldsymbol{\phi}_1 + a^3\mathbf{n}\left(\boldsymbol{\Phi}_1^3\right) \\ u_{2A} = 0, \;\; u'_{2A} = 0 \end{cases} \tag{37}$$

In order it can be solved, the known term $\mathbf{F}_2 := \{-\mathrm{d}_2 a\boldsymbol{\phi}_1 - \mathrm{d}_1^2 a\boldsymbol{\phi}_2, -\mathrm{d}_1^2 a\mathbf{M}\boldsymbol{\phi}_1 + a^3\mathbf{n}\left(\boldsymbol{\Phi}_1^3\right) - a\,(\mu\mathbf{K}_\mu + \nu\mathbf{K}_\nu)\,\boldsymbol{\phi}_1\}^{\mathrm{T}}$, must belong to the range of the operator; this *solvability condition* requires that:

$$\langle\boldsymbol{\Psi}, \mathbf{F}_2\rangle = 0 \;\; \forall\boldsymbol{\Psi} : \left(\mathbf{A}^* - \bar{\lambda}\mathbf{B}^*\right)\boldsymbol{\Psi} = \mathbf{0} \tag{38}$$

and it furnishes:

$$\mathrm{d}_1^2 a = (c_{1\mu}\mu + c_{1\nu}\nu)\,a + c_3 a^3 \tag{39}$$

where $c_{1\mu}$, $c_{1\nu}$, c_3 are real coefficients given in the Appendix. By using Eq. (39) and solving Eq. (37), it follows:

$$\begin{aligned} \mathbf{U}_2 \equiv \begin{Bmatrix} \mathbf{u}_2 \\ \mathbf{v}_2 \end{Bmatrix} = & \mathrm{d}_2 a \begin{Bmatrix} \boldsymbol{\phi}_2 \\ \boldsymbol{\phi}_1 \end{Bmatrix} + \mu a \begin{Bmatrix} \mathbf{z}_\mu \\ \hat{\mathbf{z}}_\mu \end{Bmatrix} + \\ & + \nu a \begin{Bmatrix} \mathbf{z}_\nu \\ \hat{\mathbf{z}}_\nu \end{Bmatrix} + a^3 \begin{Bmatrix} \mathbf{z}_a \\ \hat{\mathbf{z}}_a \end{Bmatrix} \end{aligned} \tag{40}$$

where $\mathbf{z}_\mu$, $\hat{\mathbf{z}}_\mu$, $\mathbf{z}_\nu$, $\hat{\mathbf{z}}_\nu$, $\mathbf{z}_a$, $\hat{\mathbf{z}}_a$ are solutions to linear problems (see Appendix). To make the solution to the

singular problem (37) unique, the normalization condition $u_{2B} = 0$ was enforced.

By using the results so far achieved, Eqs. (33_4) read:

$$\varepsilon^{3/2}: \begin{cases} \mathrm{d}_0\mathbf{u}_3 - \mathbf{v}_3 = -\mathrm{d}_3 a\boldsymbol{\phi}_1 - \mathrm{d}_1\mathrm{d}_2 a\boldsymbol{\phi}_2 - \mathrm{d}_1\mathbf{u}_2 \\ \mathbf{M}\mathrm{d}_0\mathbf{v}_3 + \mathbf{K}_0\mathbf{u}_3 + \mathbf{C}\mathbf{v}_3 = -\mathrm{d}_1\mathrm{d}_2 a\mathbf{M}\boldsymbol{\phi}_1 + \\ \quad - \mathbf{M}\mathrm{d}_1\mathbf{v}_2 - \mathrm{d}_1 a\left(\mu\mathbf{K}_\mu + \nu\mathbf{K}_\nu\right)\boldsymbol{\phi}_2 + \\ \quad + 3a^2\mathrm{d}_1 a\mathbf{n}\left(\boldsymbol{\Phi}_1^2\boldsymbol{\Phi}_2\right) \\ u_{3A} = 0, \;\; u'_{3A} = 0 \end{cases} \tag{41}$$

Its solvability condition entails:

$$2\mathrm{d}_1\mathrm{d}_2 a = \left(b_{1\mu}\mu + b_{1\nu}\nu\right)\mathrm{d}_1 a + b_3 a^2\mathrm{d}_1 a \tag{42}$$

where $b_{1\mu}$, $b_{1\nu}$, b_3 are real coefficients (see Appendix).

Finally, by coming back to the original time and quantities, Eq. (39) and Eq. (42) are recombined, furnishing:

$$\begin{aligned} &\ddot{a} - \left[b_{1\mu}\left(\mu - \mu_0\right) + b_{1\nu}\left(\nu - \nu_0\right)\right]\dot{a} - b_3 a^2\dot{a} + \\ &\quad - \left[c_{1\mu}\left(\mu - \mu_0\right) + c_{1\nu}\left(\nu - \nu_0\right)\right]a - c_3 a^3 = 0 \end{aligned} \tag{43}$$

which is the well-known bifurcation equation for double-zero bifurcation, in the Bogdanov normal form. In it, all the c's and b's coefficients depend on damping.

5.2 Bifurcation scenarios

The bifurcation equation (43) admits two equilibrium branches $a = a_s$, $\dot{a}_s = \ddot{a}_s = 0, \forall t$: (a) the trivial $a_T = 0$, which exists in the whole (μ, ν)- plane and, (b) the non-trivial:

$$a_{NT} = \pm\left[\frac{-c_{1\mu}\left(\mu - \mu_0\right) - c_{1\nu}\left(\nu - \nu_0\right)}{c_3}\right]^{1/2} \tag{44}$$

which exists in a half-plane of the parameter space. Stability of both branches is governed by the variational equation:

$$\delta\ddot{a} + I_1\left(\mu, \nu; a_s\right)\delta\dot{a} + I_2\left(\mu, \nu; a_s\right)\delta a = 0 \tag{45}$$

where:

$$\begin{aligned} I_1\left(\mu, \nu; a_s\right) &:= -\left[b_{1\mu}\left(\mu - \mu_0\right) + b_{1\nu}\left(\nu - \nu_0\right) + \right. \\ &\quad \left. + b_3 a_s^2\right] \\ I_2\left(\mu, \nu; a_s\right) &:= -\left[c_{1\mu}\left(\mu - \mu_0\right) + c_{1\nu}\left(\nu - \nu_0\right) + \right. \\ &\quad \left. + 3c_3 a_s^2\right] \end{aligned} \tag{46}$$

The trivial solution $a_s = a_T = 0$ is considered first. It loses stability through divergence at the locus $\mathcal{D} := \{(\mu, \nu)\,|I_2\left(\mu, \nu; 0\right) = 0\}$, and through Hopf bifurcation at the locus $\mathcal{H}_T := \{(\mu, \nu)\,|I_1\left(\mu, \nu; 0\right) = 0,\ I_2\left(\mu, \nu; 0\right) > 0\}$, which are found to be a straight line and a half-straight line, respectively tangent to the exact $\mathcal{D}$ and $\mathcal{H}$ loci at the double-zero point DZ.

When the non-trivial solution $a_s = a_{NT} = 0$ is considered, and use is made of Eq. (44), the divergence locus $I_2\left(\mu, \nu; a_{NT}\right) \equiv -2I_2\left(\mu, \nu; 0\right) \equiv -2c_3 a_{NT}^2 = 0$ turns out to be coincident with the line $\mathcal{D}$ previously defined, this entailing that the non-trivial solution does not undergo any other divergence, in addition to that one from which it arises. Moreover, since the stable zone lies in the half-plane $I_2\left(\mu, \nu; 0\right) > 0$, the static bifurcation is supercritical if $c_3 < 0$, and subcritical if $c_3 > 0$. In contrast, the non-trivial solution experiences a Hopf bifurcation at the half-straight line $\mathcal{H}_{NT} := \{(\mu, \nu)\,|I_1\left(\mu, \nu; a_{NT}\right) = 0,\ I_2\left(\mu, \nu; a_{NT}\right) > 0\}$. The inequality entails the existence condition $c_3 < 0$; if this is the case, $\mathcal{H}_T$ and $\mathcal{H}_{NT}$ lie in the half planes $I_2\left(\mu, \nu; 0\right) > 0$ and $I_2\left(\mu, \nu; 0\right) < 0$, respectively, which are separated by the line $\mathcal{D}$.

The previous qualitative analysis highlighted the strong dependence of the bifurcation scenario on the sign of the coefficient c_3. In order to investigate the influence of damping, this coefficient has been evaluated for different values of α and β, and results displayed in Table 1. It is seen that, $c_3 < 0$ when β is fixed at a small value (weakly externally damped systems) and α is varied on a range; in contrast, the coefficient changes sign when β is sufficiently large (strongly externally damped systems). A similar analysis carried out on the coefficient b_3 shows that this coefficient is always negative, this entailing that the Hopf bifurcation is always supercritical.

Guided by these results, two sample system have been considered, exhibiting supercritical and subcritical static bifurcation, respectively:

(S1) for which $\alpha = 0.01$, $\beta = 0.1$, entailing $\mu_0 = 2.806$, $\nu_0 = 2.884$ and $c_{1\mu} = -10.641$, $c_{1\nu} = 6.907$, $c_3 = -29.707$, $b_{1\mu} = 0.246$,

Table 1. Coefficient c_3 in the bifurcation equation vs. damping coefficients α and β.

$\beta = 0.1$		
$\alpha = 0.01$	$\alpha = 0.05$	$\alpha = 0.1$
-29.707	-35.669	-30.692
$\alpha = 0.3$	$\alpha = 0.8$	$\alpha = 1.5$
-12.033	-2.348	-0.703
$\alpha = 0.01$		
$\beta = 0.25$	$\beta = 0.3$	$\beta = 0.5$
-3.221	8.544	62.603
$\beta = 1$	$\beta = 5$	$\beta = 10$
235.510	958.717	574.504

$b_{1\nu} = 0.127$, $b_3 = -6.077$.

(S2) for which $\alpha = 0.01$, $\beta = 10$, entailing $\mu_0 = 3.076$, $\nu_0 = 5.302$ and $c_{1\mu} = -22.324$, $c_{1\nu} = -5.156$, $c_3 = 574.504$, $b_{1\mu} = 4.522$, $b_{1\nu} = 6.014$, $b_3 = -1153.303$.

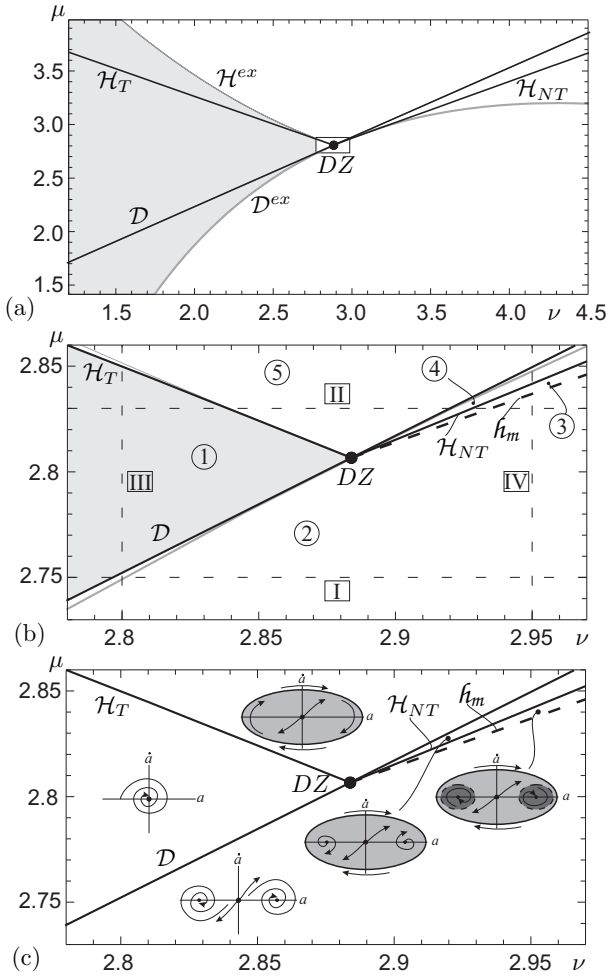

Figure 5. Bifurcation chart for system S1 in the parameter plane: (a) large view around the double-zero point and exact and asymptotic bifurcation loci; (b) small neighborhood around the bifurcation point; (c) sketches of the phase-plan in the different regions; h_m homoclinic bifurcation locus.

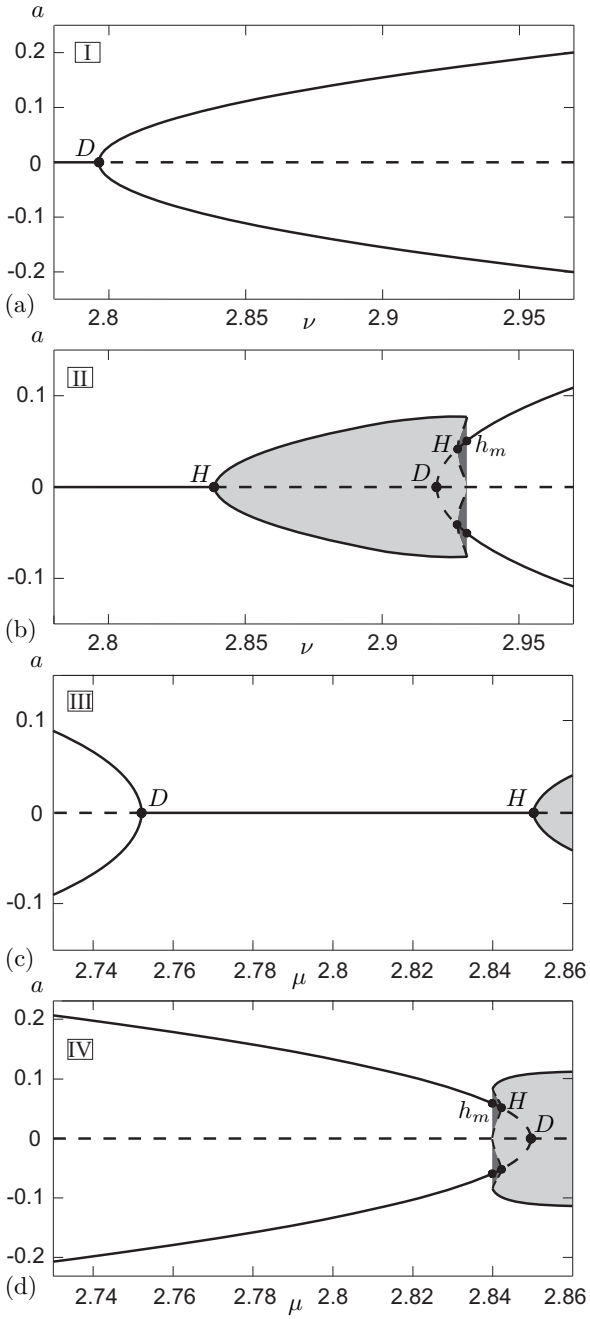

Figure 6. Bifurcation diagrams for system S1; path I to IV marked in Fig. 5_b; stable (continuous lines) and unstable (dashed lines) equilibria and cycles (shaded diagrams); labels D, H, h_m denote divergence, Hopf and homoclinic bifurcation points.

Results relevant to S1 are reported in Fig. 5, displaying the bifurcation chart, and Fig. 6, illustrating bifurcation diagrams, these latter having been obtained by a numerical continuation procedure. Figure 5_a shows a large view of the neighborhood of the double-zero point; here the tangency between asymptotic and exact bifurcation loci can be appreciated. Figure 5_b is a zoom of a small region (also marked in Fig. 5_a) in which exact loci can be confused with their tangents. Finally, Figure 5_c depicts, in each significant region, sketches of the two-dimensional phase-plane $(a, \dot{a})$ for the bifurcation equation (43). In region 1 the trivial solution is stable; due to the supercritical static bifurcation, it loses stability in region 2, where two (buckled) stable nontrivial equilibria take place; due to supercritical Hopf bifurcation, it loses stability in region 5, where a (large) stable limit cycle exists, causing periodic motion of the beam. In region 4 two equilibria appear, but, in spite of the supercritical character of the static bifurcation, they are unstable, as an effect of the interaction with the dynamic bifurcation; in region 3 two small unstable limit cycles arise (denoting periodic motions around the buckled configurations),

which render stable the nontrivial equilibria. Then, at the straight line h_m, a homoclinic bifurcation occurs (caused by the contact of the small cycles with the trivial equilibrium and, simultaneously, with the large cycles); after that, all cycles disappear, so that only stable equilibria survive in region 2. Figure 6 shows the bifurcation diagrams relevant to the paths I to IV marked in Fig. 5$_b$; labels D, H, h_m denote divergence, Hopf and homoclinic bifurcation, respectively. Path I shows the static bifurcation, from which stable nontrivial equilibria arise. Path II displays, in sequence, (a) the Hopf bifurcation from the trivial solution, leading to the appearance of large cycles, whose amplitude range is shadow in the figure; (b) the static bifurcation, leading to initially unstable nontrivial equilibria; (c) the Hopf bifurcation from the nontrivial equilibria, leading to the appearance of small cycles and the simultaneous regain of stability of the nontrivial equilibria; (d) the homoclinic bifurcation, causing the disappearing of all the cycles. Path III illustrates the loss of stability of the trivial equilibrium through divergence (for small μ) or Hopf bifurcation (for large μ). Finally, path IV shows the transition from nontrivial equilibria to large limit cycles, passing through homoclinic bifurcation. As a final comment on the scenario relevant to S1, there exist an attractor in any region, namely: one or two equilibria in regions 1 and 2, one cycle in regions 4 and 5, and two equilibria and a cycle in region 3. Therefore the bifurcation is not catastrophic. On the other hand, the regions (3 and 4) in which static and dynamic bifurcations interact are of small extension.

Numerical results relevant to system S2 are reported in Figs. 7, 8. Since $c_3 > 0$, the static bifurcation is subcritical and, according to the previous qualitative analysis, the bifurcated equilibria do not suffer Hopf bifurcation, so that no a curve $\mathcal{H}_{NT}$ exists and, consequently, no homoclinic bifurcation h_m occurs. In contrast, a new heteroclinic bifurcation h_t manifests itself. In region 1 (Fig. 7) the trivial equilibrium is stable, but two unstable equilibrium points coexist. In region 2 the trivial equilibrium loses stability by divergence, and no other local attractors exist. In region 4 the equilibrium loses stability by supercritical Hopf bifurcation, giving rise to a stable limit cycle internal to the nontrivial equilibria. In region 5, however, due to a heteroclinic bifurcation caused by the collision of cycle with the nontrivial equilibria, the cycle itself disappears. Paths I and IV (Fig. 8) show the static bifurcation; path II illustrates the succession of (a) static, (b) Hopf and (c) heteroclinic bifurcations; path III the loss of stability by divergence (small μ) or Hopf bifurcation (large μ). Therefore, system S2 has stable attractors only in region 1 (trivial equilibrium) and 4 (limit cycle); in the remaining regions no attractors exist. The bifurcation is therefore catastrophic.

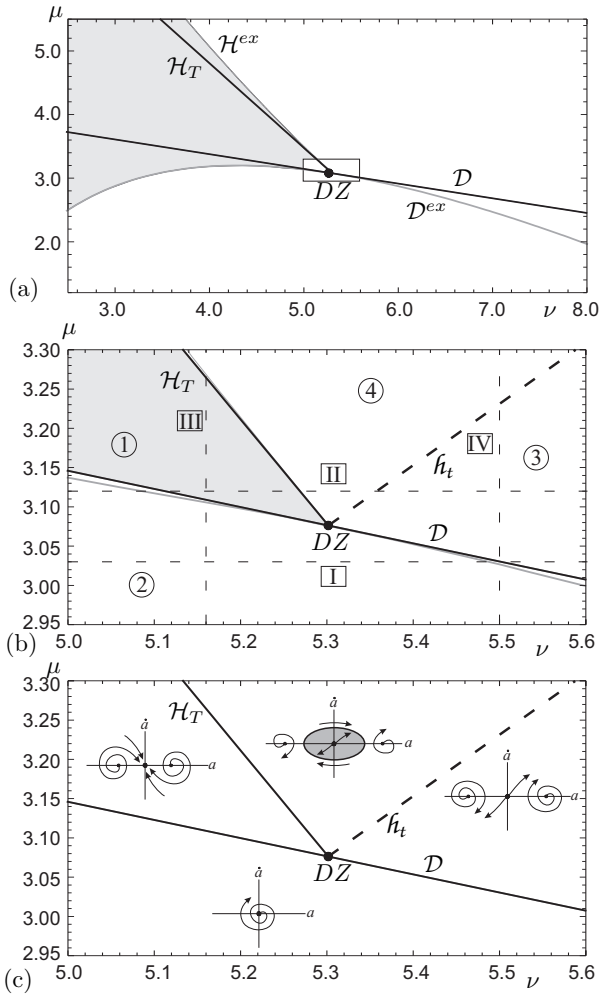

Figure 7. Bifurcation chart for system S2 in the parameter plane: (a) large view around the double-zero point and exact and asymptotic bifurcation loci; (b) small neighborhood around the bifurcation point; (c) sketches of the phase-plan in the different regions; h_t heteroclinic bifurcation locus.

6 Conclusion

A nonlinear, visco-elastic, externally dumped column, subjected to two independent axial loads, one gravitational, the other tangential, has been studied. By enforcing internal kinematical constrains, a single nonlinear integro-differential equation of motion in the transversal displacement field has been derived, equipped with proper boundary conditions. The linear stability diagram of the trivial equilibrium has been studied in detail in the plane of the two loading parameters, both for tensile and compressive forces. The existence of divergence and Hopf bifurcations has been highlighted, leading to double-zero (Takens-Bogdanov) bifurcations. A nonlinear bifurcation analysis, based on a fractional-power version of the Multiple Scale Method, has been performed around the double-zero point, by directly attacking the continuous problem (i.e. by avoiding any *a priori* discretization). An extensive parametric analysis has been carried out, with the aim to investigate the role of damping on such a

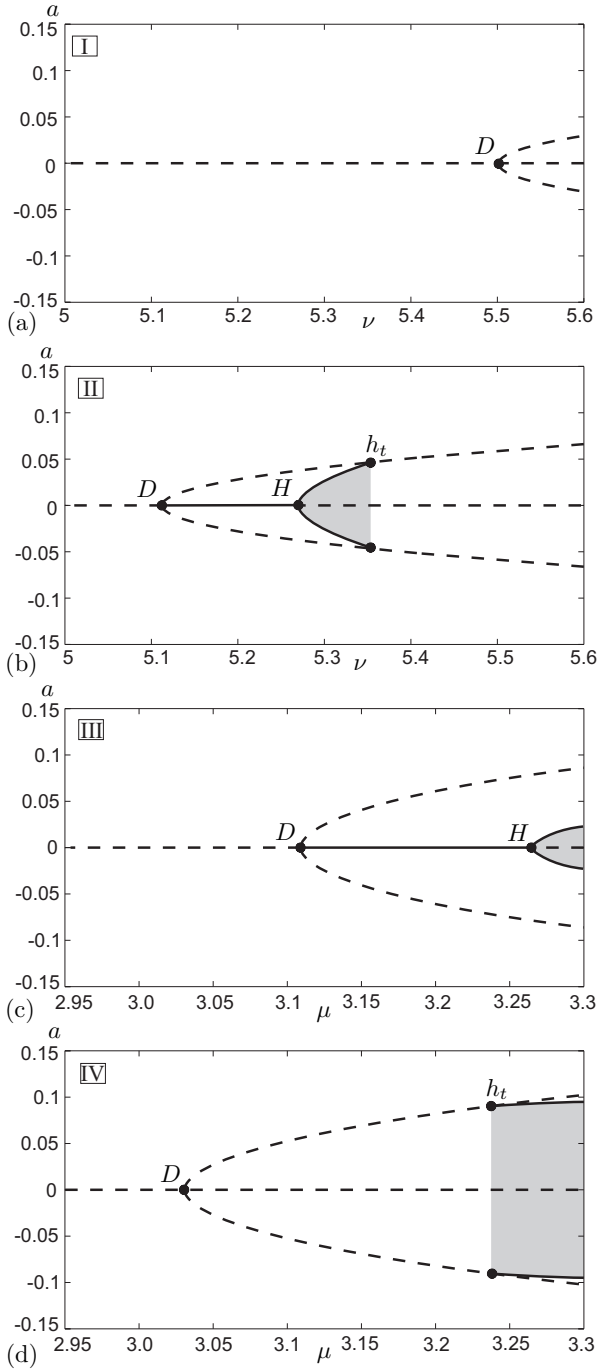

Figure 8. Bifurcation diagrams for system S2; path I to IV marked in Fig. 7_b; stable (continuous lines) and unstable (dashed lines) equilibria and cycles (shaded diagrams); labels D, H, h_t denote divergence, Hopf and heteroclinic bifurcation points.

codimension-2 bifurcation, both in linear and nonlinear problems. The following main conclusions are drawn.

1. The position of the bifurcation point and the angle of attack between the incident, divergence and Hopf, bifurcation loci depend on the damping coefficients. However, when one of the coefficients is zeroed and the other is rendered small, the properties of the undamped (circulatory) system are recovered only for evanescent external damping, not for internal damping, this case being *in discontinuity* with the circulatory case. Therefore, some new features of the well-known "destabilization paradox" are revealed.
2. Also the nonlinear scenario around the double-zero bifurcation is strongly affected by damping. When the external damping is small, the static bifurcation is *supercritical*, this entailing the existence of one or more attractor, equilibria o limit cycles, in the whole neighborhood. In contrast, when the external damping is large, the static bifurcation is *subcritical*, this entailing a catastrophic character of the bifurcation, for the lack of attractors in some region around the bifurcation point. In the whole range studied, instead, the Hopf bifurcation has supercritical character.
3. The interaction between static and dynamic bifurcations manifests itself via *homoclinic* or *heteroclinic* bifurcations, due to the collision between limit cycles and equilibria, or between cycles.

Appendix

The **z**-solutions appearing in equation (40) satisfy the following linear problems:

$$\begin{cases} \mathrm{d}_0\mathbf{z}_\mu - \hat{\mathbf{z}}_\mu = -c_{1\mu}\boldsymbol{\phi}_2 \\ \mathbf{M}\mathrm{d}_0\hat{\mathbf{z}}_\mu + \mathbf{K}_0\mathbf{z}_\mu + \mathbf{C}\hat{\mathbf{z}}_\mu = -c_{1\mu}\mathbf{M}\boldsymbol{\phi}_1 - \mathbf{K}_\mu\boldsymbol{\phi}_1 \\ z_{\mu A} = 0, \;\; z'_{\mu A} = 0 \end{cases}$$
$$\begin{cases} \mathrm{d}_0\mathbf{z}_\nu - \hat{\mathbf{z}}_\nu = -c_{1\nu}\boldsymbol{\phi}_2 \\ \mathbf{M}\mathrm{d}_0\hat{\mathbf{z}}_\nu + \mathbf{K}_0\mathbf{z}_\nu + \mathbf{C}\hat{\mathbf{z}}_\nu = -c_{1\nu}\mathbf{M}\boldsymbol{\phi}_1 - \mathbf{K}_\nu\boldsymbol{\phi}_1 \\ z_{\nu A} = 0, \;\; z'_{\nu A} = 0 \end{cases}$$
$$\begin{cases} \mathrm{d}_0\mathbf{z}_a - \hat{\mathbf{z}}_a = -c_3\boldsymbol{\phi}_2 \\ \mathbf{M}\mathrm{d}_0\hat{\mathbf{z}}_a + \mathbf{K}_0\mathbf{z}_a + \mathbf{C}\hat{\mathbf{z}}_a = -c_3\mathbf{M}\boldsymbol{\phi}_1 + \mathbf{n}\left(\boldsymbol{\Phi}_1^3\right) \\ z_{aA} = 0, \;\; z'_{aA} = 0 \end{cases} \tag{A.1}$$

under the normalization conditions:

$$z_{\mu B} = 0, \quad z_{\nu B} = 0, \quad z_{aB} = 0 \tag{A.2}$$

Due to their cumbersome expressions, they are not reported here.

Coefficients in equation (43) take the following forms:

$$\begin{aligned} c_{1\mu} &= -2\int_0^1 \psi_2\phi_1''\mathrm{d}s \\ c_{1\nu} &= -2\int_0^1 \psi_2\phi_1''\mathrm{d}s + 2\psi_{2B}\phi'_{1B} \\ c_3 &= \int_0^1 \psi_2 n_1\left(\boldsymbol{\Phi}_1^3\right)\mathrm{d}s + \psi_{2B}n_2\left(\boldsymbol{\Phi}_1^3\right) + \\ &\quad + \psi'_{2B}n_3\left(\boldsymbol{\Phi}_1^3\right) \end{aligned} \tag{A.3}$$

and:

$$
\begin{aligned}
b_{1\mu} = &- \int_0^1 \left[\left(\alpha\psi_2^{\mathrm{IV}} + \beta\psi_2\right) z_\mu + \psi_2 \hat{z}_\mu + \right. \\
&\left. + 2\psi_2\phi_2''\right] \mathrm{d}s + \alpha\psi_{2B}''' z_{\mu B} - \alpha\psi_{2B}'' z_{\mu B}' \\
b_{1\nu} = &- \int_0^1 \left[\left(\alpha\psi_2^{\mathrm{IV}} + \beta\psi_2\right) z_\nu + \psi_2 \hat{z}_\nu + \right. \\
&\left. + 2\psi_2\phi_2''\right] \mathrm{d}s + \alpha\psi_{2B}''' z_{\nu B} - \alpha\psi_{2B}'' z_{\nu B}' + \\
&+ 2\psi_{2B}\phi_{2B}' \\
b_3 = &- 3 \int_0^1 \left(\alpha\psi_2^{\mathrm{IV}} + \beta\psi_2\right) z_a + \psi_2 \hat{z}_a + \\
&- \psi_2 n_1 \left(\mathbf{\Phi}_1^2 \mathbf{\Phi}_2\right) \mathrm{d}s + 3 \left[\alpha\psi_{2B}''' z_{aB} + \right. \\
&- \alpha\psi_{2B}'' z_{aB}' + \psi_{2B} n_2 \left(\mathbf{\Phi}_1^2 \mathbf{\Phi}_2\right) + \\
&\left. + \psi_{2B}' n_3 \left(\mathbf{\Phi}_1^2 \mathbf{\Phi}_2\right)\right]
\end{aligned}
\tag{A.4}
$$

References

Beck, M. (1952). Die Knicklast des einseiting eingespannten tangential gedrückten Stabes, *Z. Angew. Math. Phys.*, (3), pp. 225–228.

Ryu, B.R., Katayama, K., Sugiyama, Y. (1998). Dynamic stability of Timoshenko columns subjected to subtangential forces, *Comput. Struct.*, (68), pp. 499–512.

Langthjem, M. A., Sugiyama, Y. (2000). Dynamic stability of columns subjected to follower loads: A survey., *J. Sound. Vib.*, **238**(5), pp. 809–851.

Detinko, F.M. (2003). Lumped damping and stability of Beck column with a tip mass, *Int. J. Solids. Struct.*, (40), pp. 4479–4486.

Kirillov, O.N., Seyranian, A.P. (2005). The effect of small internal and external damping on the stability of distributed non-conservative systems, *J. Appl. Math. Mech.*, (69) pp. 529–552.

Ziegler, H. (1952). Die Stabilit/itskriterien der Elastomechanik. *Ing.-Arch.*, **20**(1), pp. 49–56.

Bolotin, V. V., Zhinzher, N. I. (1969). Effects of damping on stability of elastic systems subjected to non-conservative forces, *Int. J. Solids. Struct.*, **5**(9), pp. 965–989.

Andreichikov I. R, Yudovich, V. I. (1974). The stability of visco-elastic rods, *Izu. Akad. Nauk SSSR. MTT*, (2), pp. 78–87.

Denisov, G. G., Novikov, V. V. (1975). The stability of a rod loaded by a "follower" force., *Izv. Akad. Nauk SSSR. MTT*, (1), pp. 150–154.

Seyranian, A. R. (1990). The destabilization paradox in stability problems for non-conservative systems, *Usp. Mekh.*, **13**(2), pp. 89–124.

Kirillov, O. N. (2004). The destabilization paradox, *Dokl. Ross. Akad. Nauk*, **395**(5), pp. 614–620.

Langthjem, M. A., Sugiyama, Y. (2000). Optimum design of cantilevered columns under the combined action of conservative and nonconservative loads: Part I: The undamped case, *Comput. Struct.*, **74**(4), pp. 385–398.

Adali, S. (1982). Stability of a rectangular plate under nonconservative and conservative forces, *Int. J. Solids. Struct.*, **18**(12), pp. 1043–1052.

Troger, H., Steindl, A., (1991). *Nonlinear Stability and Bifurcation Theory*, Appendix L, pp. 366–375 Springer, Wien, New York.

Luongo, A., Di Egidio, A., Paolone, A. (2002). Multiple scale bifurcation analysis for finite-dimensional autonomous systems, in: *Recent Research Developments in Sound and Vibration*, (1), Transworld Research Network, Kerala, India, ISBN:81-7895-031-6 pp. 161–201.

Luongo, A., Di Egidio, A. (2005). Bifurcation equations through multiple-scale analysis for a continuous model of a planar beam, *NonLinear Dynam.*, (41), pp. 171–190.

Di Egidio, A., Luongo, A., Paolone, A. (2007). Linear and non-linear interactions between static and dynamic bifurcations of damped planar beams, *Int. J. Nonlinear Mech.*, (42), pp. 88–98.

Luongo, A.., Di Egidio, A. (2006). Divergence, Hopf and Double-Zero Bifurcations of a Nonlinear Planar Beam, *Comput. Struct.*, (84), pp. 1596–1605.

Luongo, A., Paolone, A., Di Egidio, A. (2000). Sensitivities and linear stability analysis around a double zero eigenvalue, *AIAA Journal*, **38**(4), pp. 702–710.